OSU Oregon State University

Open Access Articles

Wireless, Low-Cost, FPGA-based Miniature Gamma Ray Spectrometer

The Faculty of Oregon State University has made this article openly available.
Please share how this access benefits you. Your story matters.

Citation	Becker, E. M., & Farsoni, A. T. (2014). Wireless, low-cost, FPGA-based miniature gamma ray spectrometer. Nuclear Instruments and Methods in Physics Research Section A: Accelerators, Spectrometers, Detectors and Associated Equipment, 761, 99-104. doi:10.1016/j.nima.2014.05.096
DOI	10.1016/j.nima.2014.05.096
Publisher	Elsevier
Version	Accepted Manuscript
Terms of Use	http://cdss.library.oregonstate.edu/sa-termsofuse

Oregon State University OSU

Wireless, Low-Cost, FPGA-based Miniature Gamma Ray Spectrometer

E. M. Becker, A. T. Farsoni

Department of Nuclear Engineering and Radiation Health Physics,
Oregon State University, Corvallis, OR 97331, USA

Abstract

A compact, low-cost, wireless gamma-ray spectrometer is a tool sought by a number of different organizations in the field of radiation detection. Such a device has applications in emergency response, battlefield assessment, and personal dosimetry. A prototype device fitting this description has been constructed in the Advanced Radiation Instrumentation Laboratory at Oregon State University. The prototype uses a CsI(Tl) scintillator coupled to a solid-state photomultiplier and a 40 MHz, 12-bit, FPGA-based digital pulse processor to measure gamma radiation, and is able to be accessed wirelessly by mobile phone. The prototype device consumes roughly 420 mW, weighs about 28 g (not including battery), and measures 2.54 x 3.81 cm^2. The prototype device is able to achieve 5.9% FWHM energy resolution at 662 keV.

Keywords: Silicon Photomultiplier, Scintillator, Digital Pulse Processor, FPGA, Compact, Low-Cost, Gamma Ray Spectroscopy

1. Introduction

In the wake of the Fukushima accident in 2011, a large demand arose for a small, low-cost radiation detection device. Such a device would be useful for such applications as radiological emergency response, border security, personal dosimetry, and battlefield assessment. The purpose of this work was to design, build, and characterize a compact, low-cost, battery-powered, wireless radiation spectrometer that could be used in the aforementioned applications.

Each different radiation detection method has its own set of advantages and disadvantages. The ideal detector for this device was one that is small, low-cost, rugged, able to operate at a low voltage bias, able to operate at room temperature, efficient for gamma ray detection, and able to perform spectroscopy. Gas-based detectors, such as Geiger-Mueller counters, can be compact, low-cost and are able to operate at room temperature. However, these devices require a high-voltage bias, have delicate components, are not efficient for high-energy gamma rays, and have no spectroscopic capability.

Another possibility is to use a semiconductor detector. Silicon diodes are small, rugged, can be operated at room temperature, and can perform energy spectroscopy, but are also expensive and not efficient for high-energy gamma ray detection. Another type of semiconductor detector is the compound semiconductor, such as CdZnTe. These detectors can be small, rugged, operate at room temperature, are efficient for gamma ray detection, and provide good energy spectroscopy capability. However, detectors such as CZT are typically expensive.

A final possibility is to use a scintillator coupled to a light-sensitive device. Scintillation materials can be small, low-cost, efficient for gamma detection, operated at room temperature, and are capable of being used in spectroscopy systems. One type of light-sensitive device is the photomultiplier tube (PMT). However, PMTs are expensive, large, delicate, and require high voltage biases. An alternative to the PMT is the silicon photomultiplier (SiPM). These devices are inexpensive, small, rugged, and typically require less than 100 V biases. Therefore, the ideal choice of detector for this spectrometer was a scintillator coupled to a SiPM. The device described herein, called the “MiniSpec”, essentially consists of this detector, the digital pulse processing electronics, and the wireless network card (WCN).

2. Device description

The MiniSpec was designed from the start to be a self-contained, wireless, and marketable radioisotope identifier. It was therefore required to contain all detection and processing electronics, interface wirelessly with any mobile phone, and be compact, lightweight, low-power, and possess an estimated full-scale production (10,000 or more units) cost of $200 USD or less.

This was accomplished by creating a small FPGA-based digital pulse processor (DPP). All components of this DPP were mounted on a custom-made printed circuit board (PCB), including the analog and digital electronics of the signal processing chain. The complete power supply architecture, which includes several voltage regulators, was also incorporated onto the PCB. This means the MiniSpec prototype requires only a single 3.7 V input to power the detector as well as the components of the analog and digital signal processing chain. The DPP, detector, and compatible wireless network card comprise the complete MiniSpec prototype device, shown in figure 1.

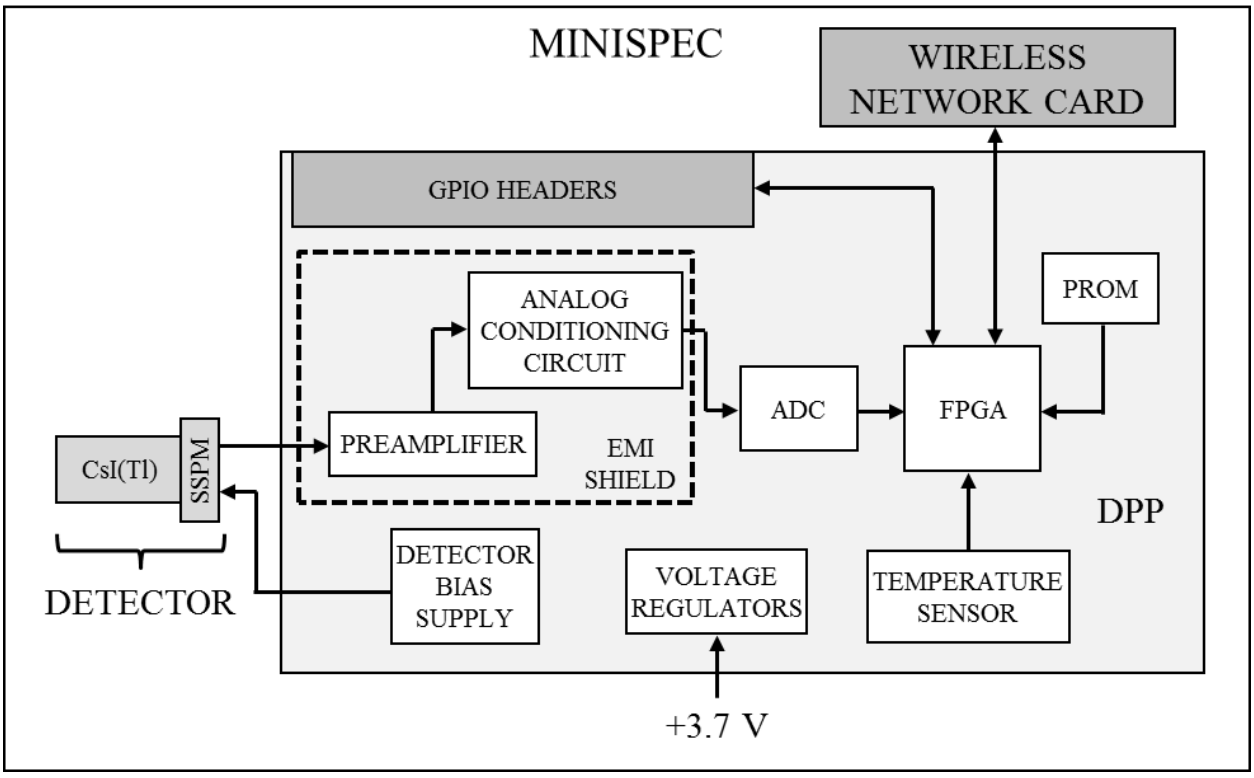

Figure 1. Diagram of the MiniSpec system.

2.1 Detector

The radiation detector chosen for the MiniSpec prototype was a SiPM coupled to a small CsI(Tl) crystal. Despite having several advantages over PMTs, listed above, the performance of SiPMs is more dependent on temperature than PMTs [1] [2]. There are ways to correct this dependence that are discussed later.

The SiPM used for the MiniSpec was the MicroSL 60035 model manufactured by SensL Technologies [3]. This model has since been replaced by the MicroSM 60000 series. The MicroSL 60035 has four 3x3 mm^2 photo-sensitive areas, each composed of 4774 microcells, giving the device 19,096 microcells total. Each microcell is an avalanche photodiode tied to a common anode and common cathode. When a photon creates electron-holes pair in a microcell, the charge carriers are accelerated by the high electric field and cause impact ionizations, which in turn causes the microcell to discharge in a manner similar to a Geiger-Mueller tube [4] [5] [6], yielding approximately the same amount of current with each discharge. Since all the microcells are connected to the same anode, the charge induced on the anode will be proportional to the number of microcells that discharge.

Ideally, each scintillation photon will trigger a different microcell, making the energy absorbed in the scintillator proportional to the amount of charge induced on the SiPM anode. However, if two or more photons are absorbed in the same microcell at the same time, the microcell will still only induce charge on the anode proportional to the absorption of one photon. They can thus become saturated when large numbers of photons are generated at a given time which causes the resulting spectrum to take on a non-linear trend. The trend of this saturation can be approximated by (1) [7]:

$$N_{fired} = M \times \left(1 - \exp\left(-\frac{PDE \times N_{ph}}{M}\right)\right), \qquad (1)$$

where N_{fired} is the number of microcells triggered, M is the maximum number of microcells, PDE is the photon detection efficiency, and N_{ph} is the number of photons incident on the sensitive area of the SiPM at a given instant. N_{ph} is dependent on the choice of scintillation material and the energy of the particle absorbed by the scintillator. A simpler equation can be applied when $M >> PDE \times N_{ph}$:

$$N_{fired} \approx PDE \times N_{ph}, \quad (2)$$

in which N_{fired} is a linear function of N_{ph}. Therefore, by using a SiPM with large number of microcells, the linear detector response with respect to energy can be extended to higher energies.

CsI(Tl) was chosen for the MiniSpec prototype for three main reasons: its high light yield per MeV, high average atomic number, and because the peak of its light emission spectrum with respect to wavelength closely matches the peak sensitivity of the SiPM. As shown in Figure 2, the peak light output of CsI(Tl) occurs at approximately 565 nm. The peak PDE of the selected SiPM occurs at approximately 500 nm, but remains relatively high at 565 nm, also illustrated in Figure 2. The CsI(Tl) crystal used in the MiniSpec was 6 x 6 x 10 mm^3 and coated in a white reflective epoxy on all sides except one of the 6 x 6 mm^2 sides. This uncoated side was coupled to the 6 x 6 mm^2 (appx.) sensitive area of the SiPM with BC-630 optical grease. These components were then wrapped tightly in Telfon tape to further reflect any scintillation light and keep the crystal centered over the sensitive area of the SiPM. This assembly was then shrouded with a custom-made light shield to block outside lighting. The separate SiPM and CsI(Tl), the wrapped assembly, and the assembly covered by the light shield can be seen in Figure 3.

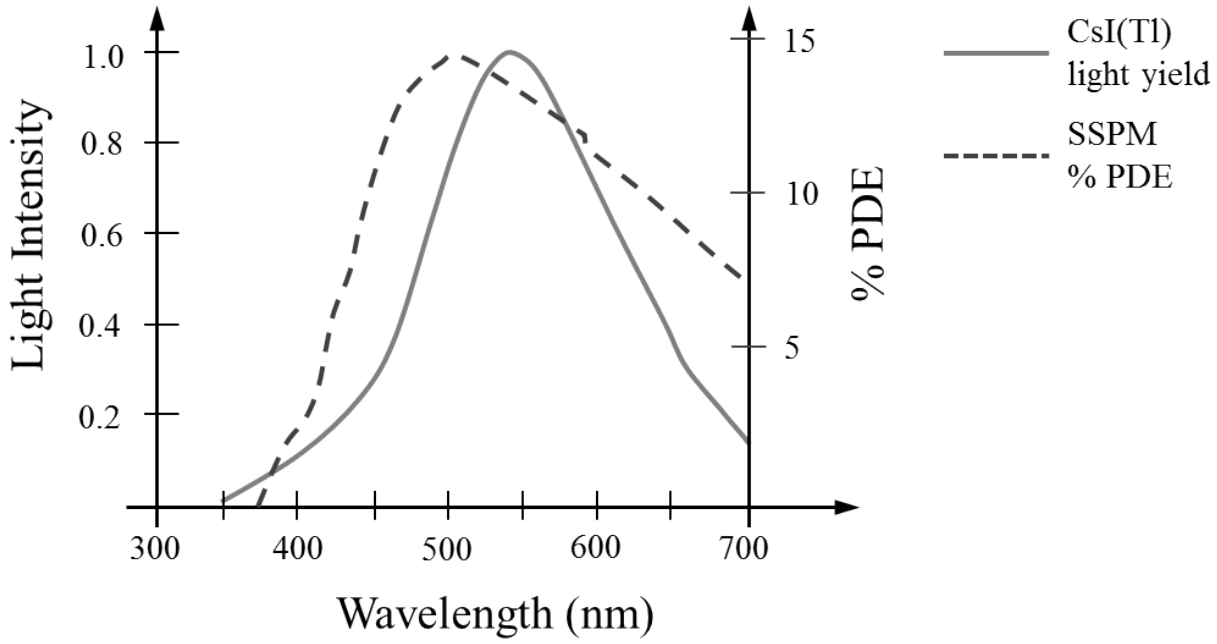

Figure 2. Illustration of CsI(Tl) light yield **[8]** and SiPM percent PDE **[3]** as a function of wavelength.

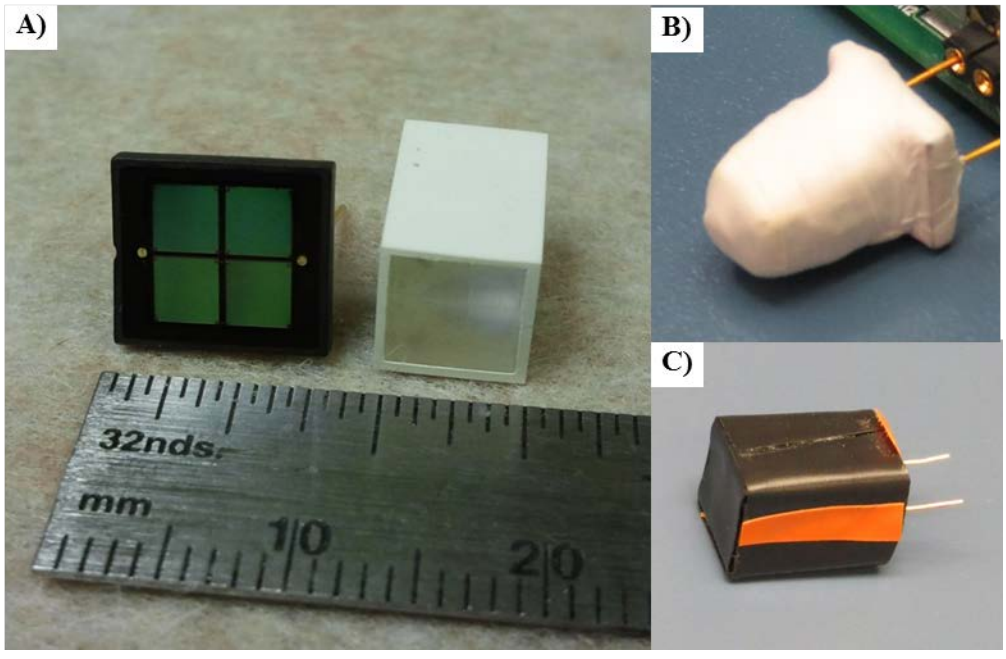

Figure 3. Pictures of A) the SiPM (left) and reflectively-coated CsI(Tl) crystal (right), B) the coupled crystal and SiPM assembly wrapped in Teflon tape, and C) the assembly inside the custom light shield.

2.2 Digital Pulse Processor

The digital pulse processor (DPP) in the MiniSpec encompasses an analog and a digital electronics section. The analog electronics are responsible for conditioning the signals from the SiPM for sampling in the digital section. Charges from the SiPM are integrated in the preamplifier and the resulting waveform passed to the analog conditioning electronics. In the analog conditioning electronics the waveform is gain-matched to the dynamic range of the ADC, and a low-pass filter is used to satisfy Nyquist requirements of the ADC sampling rate. This section is covered on the PCB by an electromagnetic interference (EMI) shield to mitigate noise induced from outside sources.

The digital section consists of the ADC and a Xilinx Spartan 6 FPGA and is responsible for sampling and processing the signal, as well as communicating with peripheral devices. The ADC has a 40 MHz sampling rate and 12-bit resolution. Digitized values are passed from the ADC directly to the FPGA where the sampled pulses are processed. A JTAG header is also included on the PCB for programming the FPGA and the external memory.

Two different operational modes can be used in the FPGA: oscilloscope mode and MCA mode. Both modes rely on a trigger module to accept valid pulses. The trigger module is based on a simple threshold-crossing algorithm using a triangular filter with a user-defined threshold. Oscilloscope mode is used to view pulse waveforms captured in one of the dual-port block-RAMs in the FPGA. In MCA mode, valid pulse waveform maxima are sampled after passing through a recursive trapezoidal shaping filter and the appropriate RAM address is incremented, generating a 4k, 32-bit energy histogram.

For prototyping purposes, three general-purpose input/output (GPIO) headers are included on the PCB for communication with peripheral devices. One peripheral device used with the MiniSpec is a USB interface board which is used in conjunction with MATLAB [9] on a PC to communicate with the MiniSpec FPGA, allowing the user to test the detection system without using the wireless interface.

2.3 Wireless Network Card

An OpenPicus Wireless Network Card (WNC) [10] was used with the MiniSpec via one of the peripheral headers mentioned in section 2.2. The WNC is shown in Figure 4 connected to the MiniSpec PCB. This card and the FPGA on the DPP communicate via several asynchronous control pins as well as a serial peripheral interface (SPI) in order to transfer data. The WNC can be operated in "ad-hoc" mode, in which it generates a WiFi signal that other devices can connect to, or in "infrastructure" mode, in which it connects to an existing WiFi network. In both modes, other devices can connect to the MiniSpec via web browser. The hosted webpage allows the user to control the operation of the MiniSpec, as well as view the energy histogram, as shown in Figure 5. This figure shows an energy spectrum from two sources captured using only the MiniSpec, with attached WNC, and a mobile phone.

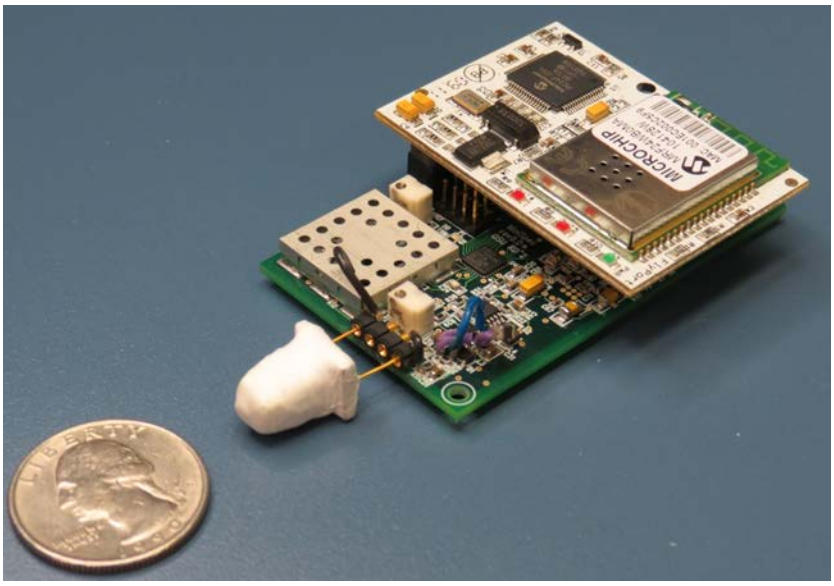

Figure 4. WNC connected to the MiniSpec PCB.

Figure 5. Mobile phone displaying gamma spectrum from ^{137}Cs and ^{22}Na sources as collected by the MiniSpec.

3. Results

3.1 Measurement Setup

Two measurement configurations were used. In measurement configuration one, the button source was placed as close as possible to the CsI(Tl) crystal in order to obtain the highest number of counts in the shortest amount of time. This configuration was used for all measurements except for full-energy peak efficiency. Measurement configuration two was only used for efficiency measurements. In this configuration, the button source was positioned 200 mm away from the front face of the CsI(Tl) crystal. This distance was chosen in order to be able to reasonably approximate the button source as a point source. Data was collected using the USB interface board and the MATLAB PC interface. Results from operation with the WNC yielded the same performance as with the USB interface board.

3.2 Noise Characterization

Noise characterization was performed by observing pulses generated by the analog conditioning electronics both with and without the detector connected and no sources present. The RMS value of the waveforms was calculated using MATLAB, and the FWHM calculated based on the RMS value. The equivalent noise contributions from the electronics with and without the detector attached were 6.15 keV(FWHM) and 0.5 keV (FWHM), respectively. The drastic increase in noise when the detector is attached could be caused by several factors. One factor is the manner of the detector attachment, which was to insert the anode and cathode leads into a connector. The noise generated by this connection can be reduced by instead soldering the SiPM to the PCB or using a SiPM designed to be surface-mounted for better connection. Another is that the detector itself generates a dark current [4] that contributes to the noise and is an intrinsic property of the detector. The detector is also unshielded, unlike the analog section of the DPP. Noise pickup in the anode and cathode leads could also contribute to the noise increase.

3.3 Energy Resolution

Energy spectra from seven different radioisotopes were collected using measurement configuration one, though not all spectra results are included here. Figure 6 shows an energy spectrum from a 0.46 μCi ^{109}Cd source. Both the 22 keV and 88 keV full-energy peaks are clearly visible. The ability to observe the 22 keV from ^{109}Cd was used to determine the value of

the trigger threshold for all measurements to ensure that the full range of spectrum features for each could be observed.

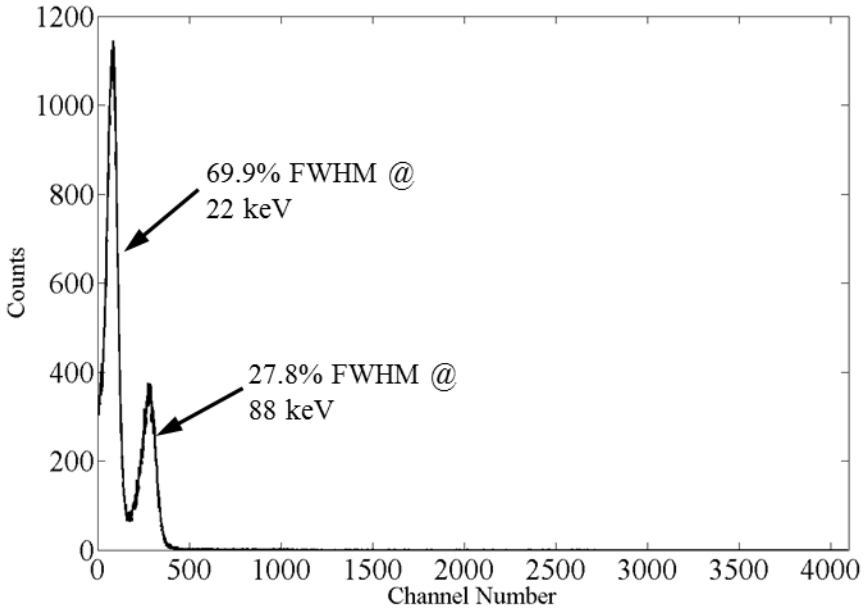

Figure 6. ^{109}Cd energy spectrum.

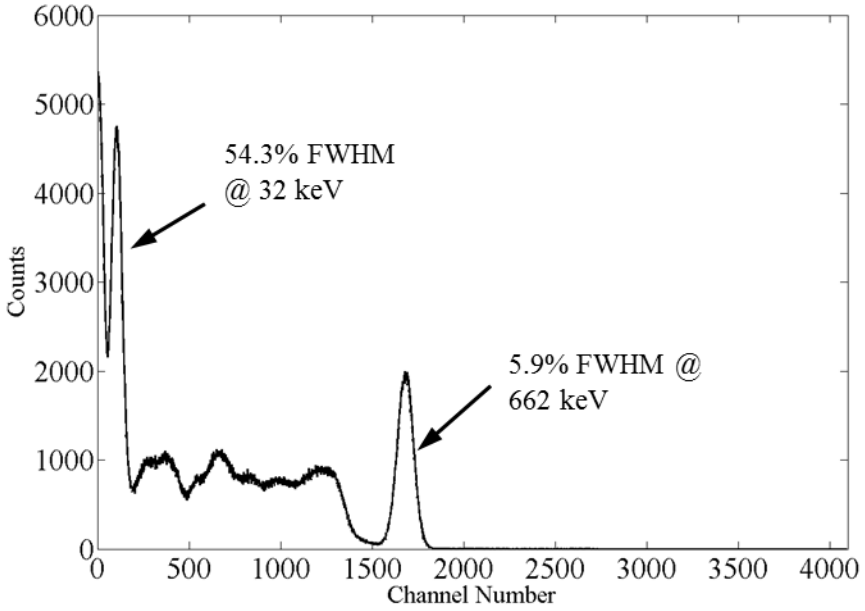

Figure 7. ^{137}Cs energy spectrum.

Figure 7 shows an energy spectrum from a 0.97 μCi ^{137}Cs source. The best recorded energy resolution for the 662 keV full-energy peak was 5.9%. This measurement was performed with the same SiPM and CsI(Tl) crystal used in previous measurements with a different set of readout electronics [11], and represents a significant improvement. Several factors may have contributed to this improvement, such as the use of the EMI shield. The 32 keV peak from characteristic X-ray is also visible in this spectrum.

Figure 8 shows the percent FWHM as a function of energy and the expected resolution trend line. In theory, the resolution should be proportional to the inverse of the square root of the number of photons generated in the CsI(Tl) [12]. However, due to the added noise of the electronics, the FWHM of the electronic equivalent noise (6.15 keV) must be considered. Taking this into account, the equation used to generate the trend line in figure 8 is Equation 3:

$$R = \frac{2.35}{\sqrt{FF \cdot PDE \cdot Y \cdot E}} + \frac{FWHM_e}{E}, \quad (3)$$

where R is the resolution, FF is the total fill factor of the [11], PDE is the photon detection efficiency of the SiPM [3], Y is the light yield per MeV of the CsI(Tl) crystal [13], E is the full-energy peak centroid, and $FWHM_e$ is the electronic FWHM.

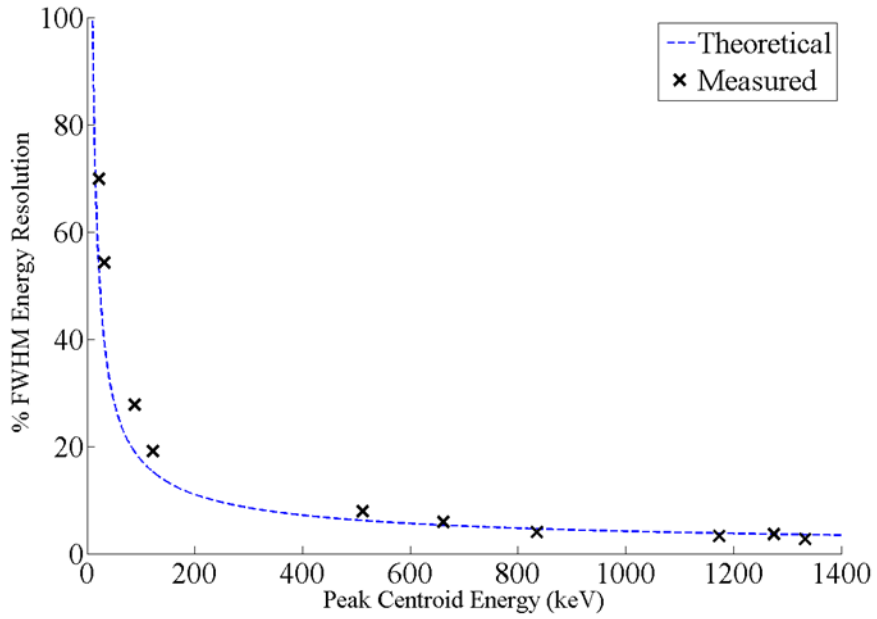

Figure 8. Percent FWHM energy resolution as a function of full-energy peak centroid with theoretical resolution fit.

3.4 Linearity and Dynamic Range

The linearity of the SiPM response to photons from the CsI(Tl) crystal was determined using the full-energy peak centroids measured in section 3.3. Figure 9 shows the channel number of the peak centroid as a function of the energy of the peak centroid, as well as two trend lines. The linear trend line is based on Equation 2 for the four lowest peak energy centroids. Higher energy peak centroids diverge significantly from this linear trend, as expected for SiPM devices. The

second trend line is based on Equation 1. Since the number of microcells fired in these measurements is unknown, a factor of k was introduced to Equation 1 to convert the number of microcells fired into the channel number at which the peak centroid is located, yielding Equation 4:

$$C_{peak} = kM \times \left(1 - \exp\left(-\frac{PDE \times N_{ph}}{kM}\right)\right), \quad (4)$$

where C_{peak} is the location of the peak centroid in terms of MCA channels. The conversion factor k is empirical based on the channel numbers of the measured peak centroids. N_{ph} is calculated by multiplying the photon yield per MeV by the expected gamma energy, and PDE is multiplied by the fill-factor of the SiPM. The saturation trend line shown in Figure 9 was generated using Equation 4. The measurements at higher energies follow the saturation trend much more closely, which indicates that the non-linearity of the MiniSpec can be primarily attributed to saturation of the microcells.

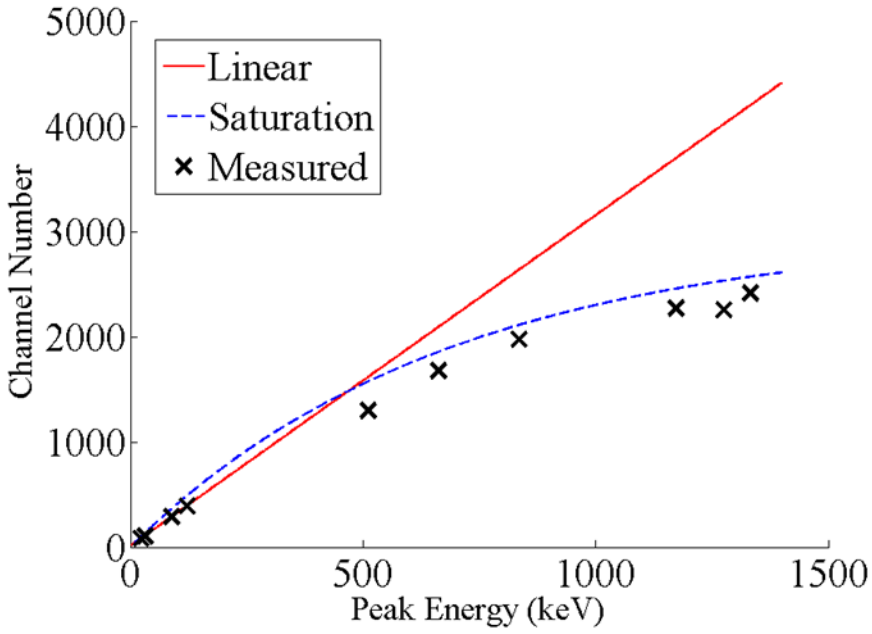

Figure 9. Channel number as a function of peak energy with linear and saturation trend lines.

The upper limit of the dynamic range of gamma rays energy able to be resolved by the MiniSpec is limited by the electronics used in the system. The dynamic range of the ADC is the main limiting factor, though components in the analog electronics section of the DPP also have input and output limits. Based on measurements made using an oscilloscope and the energy calibration generated using the saturation trend line in figure 9, the maximum energy that can be measured in the current MiniSpec configuration is 1.8 MeV.

The minimum resolvable energy is determined by the trigger threshold, which is a function of the noise level equivalent energy generated in the analog electronics. The smallest full-energy peak observed was 22 keV from ^{109}Cd at the minimum allowable threshold, making this the effective minimum resolvable energy.

3.4 Full-Energy Peak Efficiency

The full-energy peak intrinsic efficiency [14] was measured for each full-energy peak discernible from the efficiency measurements. However, the peaks below 511 keV yielded insufficient counts compared to the background counts to accurately calculate their efficiency. Thus, their intrinsic efficiencies are therefore not calculated here. The calculated efficiencies for the other full-energy peaks are shown in Figure 10.

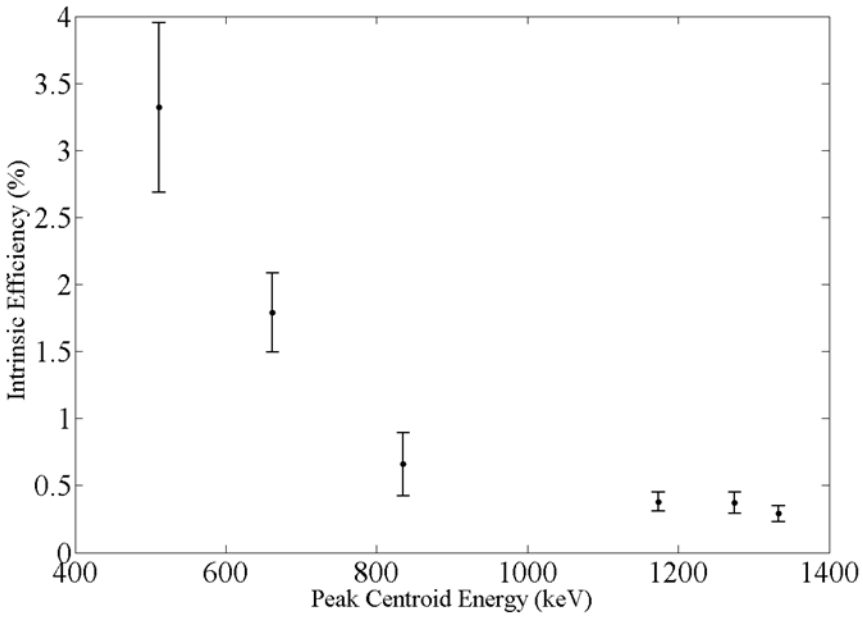

Figure 10. Measured full-energy peak efficiency.

Conclusion

A low-cost, compact gamma-ray spectrometer has been successfully designed, constructed, and characterized. This device is low-power, requiring only 420 mW from a single 3.7 V input, weighs 28 g (without battery), and is 2.54 x 3.81 cm^2. This device is able to communicate via WiFi with mobile devices via web browser, eliminating the need for a specialized application. Spectroscopic features of the MiniSpec were characterized, with a best FWHM energy resolution of 5.9% at 662 keV. The MiniSpec is able to resolve spectral features such as low-energy x-rays, backscatter peaks, and escape peaks, and has a dynamic range of 22 keV to 1.8 MeV. The intrinsic full-energy peak efficiency was measured for several energies, and was 1.79% at 662 keV. The noise of the electronics was determined to add 6.15 keV (FWHM).

The MiniSpec can be modified in several ways to add functionality and features. Perhaps the most important of these is temperature correction. A temperature sensor was built into the MiniSpec DPP for use with the MCA algorithm to adjust the channel numbers in the histogram,

but was not implemented at the time of writing. Additional features, such as linearization correction, further wireless interface development, and optimization of power resources, noise shielding, count rate optimization, and size can also be implemented to improve this device.

References

[1] M. Ramilli, "Characterization of SiPM: temperature dependencies," in *IEEE Nucl. Sci. Symp. Conf. Record*, 2008.

[2] C. Tur, V. Solovyev and J. Flamanc, "Temperature characterization of scintillation detectors using solid-state photomultipliers for radiation monitoring applications," *Nucl. Instr. Meth. A*, vol. 620, no. 2, pp. 351-358, 2010.

[3] SensL, "MicroSL Silicon Photomultiplier Detectors Datasheet," January 2012. [Online]. Available: www.sensl.com. [Accessed November 2011].

[4] SensL, "An Introduction to the Silicon Photomultiplier," 21 October 2011. [Online]. Available: http://www.sensl.com/downloads/ds/TN%20-%20Intro%20to%20SPM%20Tech.pdf. [Accessed 28 June 2013].

[5] D. Renker, "Geiger-mode avalanche photodiodes, history, properties and problems," *Nucl. Instr. Meth. A*, vol. 567, no. 1, pp. 48-56, 2006.

[6] E. Rutherford and H. Geiger, "An Electrical Method of Counting the Number of α-Particles from Radio-Active Substances," *Proc. Royal Society of London A*, vol. 81, no. 546, pp. 141-161, 1908.

[7] A. G. Stewart and et al., "Performance of 1-mm^2 Silicon Photomultiplier," *IEEE Jrnl. Quant. Elect.*, vol. 44, no. 2, pp. 157-164, 2008.

[8] Saint-Gobain Crystals, "CsI(Tl), CsI(Na), Cesium Iodide Scintillation Material," 2012. [Online]. Available: http://www.detectors.saint-gobain.com/uploadedFiles/SGdetectors/Documents/Product_Data_Sheets/CsI(Na)-CsI(Tl)-Data-Sheet.pdf. [Accessed 13 August 2013].

[9] The MathWorks, Inc., "MATLAB, v.2012b," 2013. [Online]. Available: http://www.mathworks.com/products/matlab/?s_tid=hp_fp_ml. [Accessed 04 August 2013].

[10] E. M. Becker, A. T. Farsoni, A. M. Alhawsawi and B. Alemayehu, "Small Prototype Gamma Spectrometer Using CsI(Tl) Scintillator Coupled to a Solid-State Photomultiplier," *IEEE Trans. Nucl. Sci.*, vol. 60, no. 2, pp. 968-972, 2013.

[11] Brookhaven National Laboratory, "Interactive Chart of Nuclides," [Online]. Available: http://www.nndc.bnl.gov/chart/chartNuc.jsp. [Accessed 7 July 2013].

[12] G. F. Knoll, Radiation Detection and Measurement, Hoboken, USA: John Wiley & Sons, Inc., 2000.

[13] Hilger Crystals, "Properties of CsI(Tl)," 2013. [Online]. Available: http://www.hilger-crystals.co.uk/properties.asp?material=7. [Accessed 6 July 2013].

[14] The Insitute of Electrical and Electronics Engineers, "IEEE Standard Test Procedures for Germanium Gamma Ray Detectors, ANSI/IEEE Std 325-1986," IEEE, New York, 1986.